Evolution of Primary Spacing during Directional Solidification of Transparent Bulk Samples Conducted on DECLIC-DSI

Jorge Pereda, F.L. Mota, B Billia, Y Song, Jean-Marc Debierre, A Karma, R Trivedi, N. Bergeon

Evolution of Primary Spacing during Directional Solidification of Transparent Bulk Samples Conducted on DECLIC-DSI

J. Pereda[1], F.L. Mota[1], B. Billia[1], Y. Song[2], J.M. Debierre[1], A. Karma[2], R. Trivedi[3] and N. Bergeon[1]

[1] IM2NP, Aix-Marseille Université and CNRS, Marseille, France
[2] Physics Department, Northeastern University, Boston, USA
[3] Department of Materials Science & Engineering, Iowa State University, USA

Abstract

In solidification, in situ observation of the solid-liquid interface is an invaluable tool to analyse the microstructure formation but under terrestrial conditions, convection effects dominate in bulk samples and prevent precise characterization of microstructure dynamics. The reduced-gravity environment of Space is therefore mandatory for fluid flow elimination. To study the dynamical formation of extended two-dimensional arrays of cells and dendrites in 3D samples under diffusive growth conditions, several series of microgravity experiments of directional solidification in a model transparent alloy have been conducted onboard the International Space Station using the Directional Solidification Insert (DSI) of the Device for the Study of Critical Liquids and Crystallization (DECLIC) facility. This facility was developed by the French Space Agency (CNES) in collaboration with NASA. In such large samples, the situation of a single crystal ideally orientated with a perfectly flat interface is out of reach. Analyses revealed the presence of numerous subboundaries that competitive growth processes, even in a cellular regime. The influence of subboundary configuration on the dynamics of primary spacing selection will be here evidenced.

Keywords: directional solidification, pattern formation, transparent alloys.

1. Introduction

Directional solidification experiments under low gravity conditions provide a unique framework to investigate microstructure development in spatially extended sample geometries, with negligible convection effects and under well-controlled conditions of growth rate, temperature gradient, and alloy composition. The study presented here was conducted using the DSI (Directional Solidification Insert) of the DECLIC facility (Device for the Study of Critical Liquids and Crystallization), developed and operated by the French Space Agency CNES and NASA. It is dedicated to in situ and real time characterization of the dynamical selection of the solid-liquid interface morphology in bulk samples of transparent materials.

Those experiments provide unique benchmark data to validate the predictions of theoretical and computational models in a purely diffusive growth regime. Removing convection enables to obtain more homogeneous patterns [1], providing ideal conditions to unprecedented observations, as demonstrated with the characterization of extended 2D oscillating cellular patterns [2-4].

In this paper, we will present some elements of analysis of the primary spacing evolution from triggering of morphological instability to steady-state. In such large samples, the situation of a single crystal ideally orientated with a perfectly flat interface is out of reach. After a brief description of the experimental procedure, results will be described and discussed in terms of pattern formation and evolution. We will attach to highlight the influence of subboundaries on spacing selection.

2. Experimental procedure

Essentially, the DECLIC-DSI insert consists of two elements: the Bridgman furnace and the experimental cartridge.

The experimental cartridge includes a quartz crucible and a system of volume compensation made of stainless steel that is useful to accommodate the sample volume variations associated to phase changes. The cylindrical crucible has an inner diameter of ten millimeters and a length that enables about ten centimeters of solidification, allowing the study of the entire development of the microstructure, from the initial stage to the steady state.

The crucible is equipped with a flat glass window at the bottom and a lens immersed in the melt at the top.

The cartridge was filled under vacuum with a succinonitrile (SCN) – 0.24 wt% camphor alloy, using SCN purified by NASA through distillation and zone melting. Once sealed, the cartridge was inserted in the Bridgman furnace. A monocrystalline seed with a direction ‹100› parallel to the pulling axis was prepared on ground and kept unmelted during all the experimental campaign.

The hot and cold zones of the Bridgman furnace were setup in a way to impose a thermal gradient ranging from 10 to 30 K/cm and to maintain the solid-liquid interface in the adiabatic area located between the cold and hot zones. Experiments presented in this paper were done at G = 19 K/cm [5]. During the experiment, the crucible is pulled down from the hot zone into the cold zone at a rate V_P ranging from 0.1 to 30 µm/s.

A schematic of the optical diagnostics is given in Figure 1. The experimental cartridge is reduced to a cylinder with liquid on top and solid at the bottom. The main observation mode (axial observation) takes advantage of the complete axial transparency of the cartridge: the light coming from LEDs passes through the cartridge from the bottom to the top, therefore crossing the interface. The optical imaging system formed by the immersed lens and a following relay lens forms the image of the interface on a CCD camera. On the same cartridge axis, a He-Ne Mach-Zehnder interferometer is also present (detailed in [6,7]). The interface can also be observed from the side (transverse observation detailed in [5]).

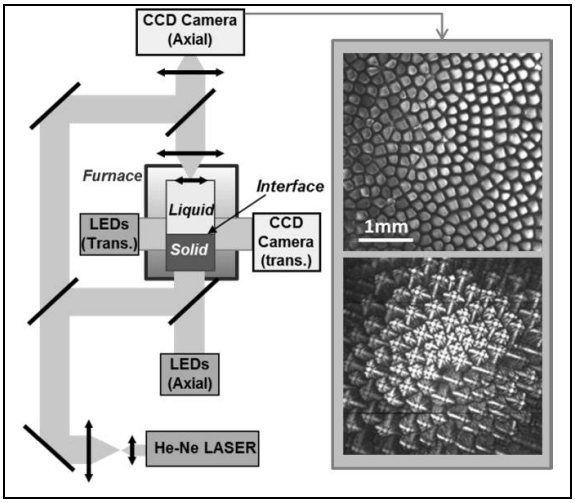

Figure 1: Schematic of the optical diagnostics of the DECLIC-DSI.

The resulting raw data are a sequence of images of the interface during solidification, including the onset and stabilization of the solidification front. To study the microstructural evolution of the solidification interface, each cell is characterized in terms of its position on the interface and its size. The labels of each cell are associated across images, so that one cell can be followed through the successive images, and its creation, movement, and elimination followed. In this paper, we will focus on the primary spacing evolution, defined as the centre-to-centre distance between neighbouring cells.

3. Results

3.1 Evidencing subboundaries

As mentioned earlier, we started the experimental campaign with a single crystal, with a ‹100› direction aligned with the pulling axis as closely as possible, and only the very top of the solid seed was remelted. But it rapidly appeared that subboundaries were present, probably due to dislocation reorganizations, inducing seed crystal polygonization.

It is long known that defects such as grain boundaries or subboundaries play a critical role in initiating morphological instability [8,9]. Depending on growth conditions, those subboundaries can then be evidenced by the earlier birth of morphological instability localized on these subboundaries. Figure 2 illustrates this observation for the first stage of the development of a cellular pattern. As already observed by Noël et al [9], the very nice and particular arrangement of cells along the grain boundary disappears with time so that subboundaries are no longer visible.

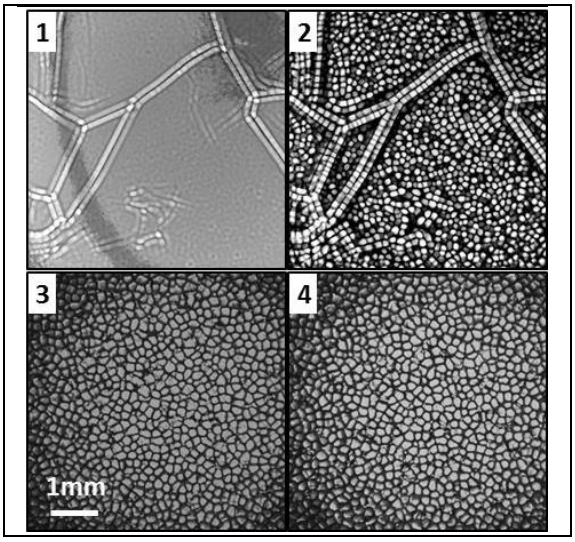

Figure 2: Development of morphological instability initiating on subboundaries. Once the pattern is well developed, subboundaries are no longer visible. t_1 = 1.6h, t_2 = 1.8h, t_3 = 2.7h, t_4 = 4h (V_P = 1 µm/s ; G = 19 K/ cm)

Locating subboundaries in a well-developed pattern is thus more complicated. The growth direction of a cell/dendrite changes from the thermal gradient direction at low velocity to the closest ‹100› direction when pulling rate increases [10,11], meaning that the growth direction will be misorientated with respect to the pulling/thermal axis if no ‹100› direction is perfectly aligned with this axis. If the misalignment between the preferred growth direction ‹100› and the pulling/thermal axis is large enough, structures are tilted compared to the optical axis, and this may help to distinguish subgrains. In cellular regime, most of the time, no obvious microstructural

difference between subgrains is observed since the effects of misorientation decrease when the pulling velocity decreases. In that case, trajectories of cells are analysed: each subgrain is characterized by a collective drift of cells, of specific direction and amplitude, caused by the misalignment between the growth direction and the pulling/thermal axis. Due to small misorientations, both directions and amplitudes are required to discriminate the subgrains and several successive images may be used to validate the location of boundaries. This type of analysis will be conducted in §2.3.

3.2 Primary spacing evolution

The evolution of spacing was measured as a function of time for each pulling rate. Two examples of such data are given in Figure 3 with the spacing variation as a function of solidified length (namely the "pulling length" = $V_P \times t$), for V_P = 0.5 µm/s and V_P = 4 µm/s. At the very beginning of microstructure formation, it is not possible to determine the spacing with center-to-center methods as microstructure does not form distinct cells. Therefore the first measurements are performed using a FFT (Fast Fourier Transform) based method. At low pulling velocity (for example 0.5 µm/s), the spacing progressively increases to reach its steady-state value. At higher velocity (for example 4 µm/s), the spacing displays an overgrowth of cells at the beginning of solidification before a slow decrease to reach a steady-state value; this dynamics is consistent with previous observations on thin samples of succinonitrile-based alloys, for example by Seetharaman et al.[12]. The overgrowth appears from V_P = 2 µm/s. The detailed observation of the first stages of pattern formation revealed a transition at this pulling rate in the birth of instability mode: below 2 µm/s, instability develops primarily subboundaries and later inside subgrains, whereas above 2 µm/s, instability develops homogeneously along the interface, including simultaneously subboundaries. Such observations are similar to Noël et al. [9] ones. Moreover, the analysis of several experiments performed at the same pulling rate revealed that the amplitude of the overgrowth slightly increases when instability triggers a little bit earlier. The overgrowth could be related to an early birth of instability. These elements still need to be clarified with a deeper characterisation of the birth of morphological instability in terms of time, size and location.

3.3 Primary spacing and subboundaries

As detailed in [5], the combination of the curvature of isotherms and processes of latent heat evacuation leads to a macroscopic steady-state shape of interface generally curved, with a strong dependence on pulling rate. For the gradient G = 19 K/cm, it passes from convex at low pulling rates to concave at higher ones. As curvature is known to affect pattern dynamics [13,14], especially inducing pattern

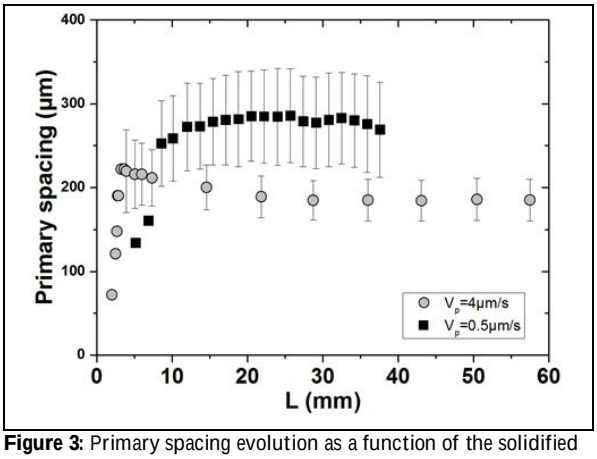

Figure 3: Primary spacing evolution as a function of the solidified length *L* for V_P = 4 µm/s and V_P = 0.5 µm/s (G = 19 K/cm).

drift, we will focus on the experiment performed at V_P = 2 µm/s to eliminate curvature influence as it corresponds to a macroscopically flat interface (transition between convex and concave cases).

In that experiment, the analysis of drifting velocity led us to identify three subgrains, as described in Figure 4a and b, with very similar gliding direction and speed, associated to convergent subboundaries (in white) and a divergent one (in black). Let us precise that the divergent boundary is associated to cell tips of both grains moving roughly in the same direction (towards the right), but cells of the rightmost grain move faster than cells in the leftmost grain.

In addition to their gliding velocity, we analyzed the primary spacing evolution of each cell. Figure 4c corresponds to the primary spacing map at the end of the coarsening stage, at the maximum of the overgrowth: primary spacing is heterogeneous, but it does not have a region-dependent structure. The average primary spacing then slowly decreases to reach its steady state value (plain curve of Figure 5). Almost no tip-splitting's are observed during this stage; numerous eliminations occur but mainly located along the convergent subboundary. The very low drifting velocities, associated to a motion of cells of the order of 1.3 mm (interface diameter: 10 mm), mean that the majority of cells initially present at the overgrowth are kept until the end of the experiment. The global and collective decrease of primary spacing is however region-dependent as observed in Figure 5 where the evolutions of the primary spacing for each subgrain are given. The difference in average primary spacing is also linked to differences of shape and extension of the distributions, as illustrated in the inset of Figure 5. Considering the very similar misorientations of subgrains associated to drifting velocities ($\theta_{growth} \cong 1.5°$), the differences can not originate in the misorientation. Therefore, the different behaviours between subgrains are attributed to the influence of boundaries: type of subboundary (divergent, associated to cells stretching, or convergent, which acts as a sink), contact with the crucible (source or sink). In particular, the second peak at large spacing's observed in the

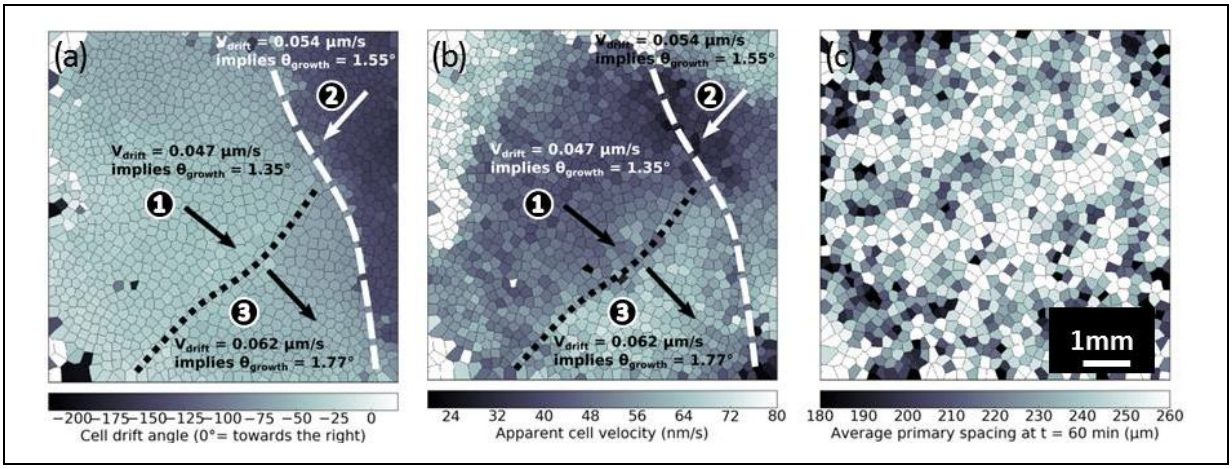

Figure 4: Analysis of the drifting velocity of cells to identify subgrains: drifting direction in a) and drifting velocity in b). 3 subgrains are identified; their average drifting velocity, direction and corresponding misorientation of the ‹100› direction with respect to the thermal/optical axis are given. c) Mapping of primary spacing of cells at t = 1h. (V_P = 2 µm/s ; G = 19 K/cm).

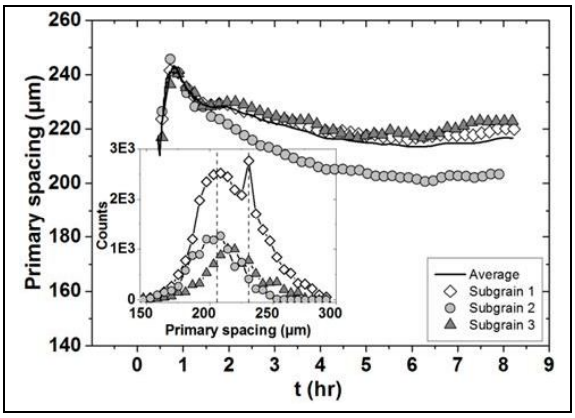

Figure 5: Primary spacing evolution: average on the whole interface, and by subgrain. The histograms correspond to the distributions by subgrain at t = 5.5h, integrated on successive images on a duration of 0.4 h (V_P = 2 µm/s; G = 19 K/cm).

distributions of subgrains 1 and 3 is due to the divergent subboundary. To be relevant, analyses and comparisons with numerical simulations must then be performed by subgrain and not on the whole interface.

4. Conclusion

We have presented here some results obtained in microgravity using the Directional Solidification Insert of the DECLIC facility on board ISS. Long solidifications were performed to get the whole dynamics and mechanisms of microstructure formation or change, spacing adjustment, pattern ordering. These microgravity experiments provided a unique opportunity to observe for the first time the formation and evolution of directionally solidified 2D extended arrays in diffusive transport conditions.

3D experiments introduce additional unavoidable deviations from ideal models of solidification, which are negligible or controllable in thin samples, and which affect the microstructure characteristics and dynamics. Complete analyses of pattern formation and spacing evolution must take into account the critical influence of the macroscopic interfacial curvature and crystalline misorientations. Thermal analyses also revealed a strong shifting of the thermal field while pulling, in contrast with the classical hypothesis of a growth in a frozen thermal field, especially during the first stages of growth and microstructure formation [5]. Understanding the influence of each of these elements is a promising challenge from both numerical and experimental points of view.

Acknowledgements

The authors express their gratitude to CNES for the support received through the MISOL3D project (MIcrostructures de SOLidification 3D), and to NASA through Grants No. NNX16AB54G and No. NNX12AK54G.

References

1. N. Bergeon *et al.*, *Int. J. Microgravity Sci. Appl.*, 2016, **33**: 330207.
2. N. Bergeon *et al.*, *Phys. Rev. Lett.*, 2013, **110**: 226102.
3. D. Tourret *et al.*, *Phys. Rev. E*, 2015, **92**: 042401.
4. J. Pereda *et al.*, *Phys. Rev. E*, 2017, **95**: 012803.
5. F. L. Mota *et al.*, *Acta Mater.*, 2015, **85**: 362.
6. H Jamgotchian *et al.*, *Journal of Microscopy-Oxford*, 2001, **203**: 119.
7. N. Bergeon *et al.*, *Trans. IIM*, 2009, **62**: 455.
8. R.J. Schaefer *et al.*, *Metall. Trans.*, 1970, **1**: 1973.
9. N. Noel *et al.*, *J. Cryst. Growth*, 1998, **187**: 516.
10. S. Akamatsu *et al.*, *Phys. Rev. E*, 1997, **56**: 4479.
11. J. Deschamps *et al.*, *Phys. Rev. E*, 2008, **78**: 011605.
12. V. Seetharaman *et al.*, *Acta Metall.*, 1988, **36**: 1175.
13. C. Weiss *et al.*, *Phys. Rev. E*, 2009, **79**: 011605.
14. S. Bottin-Rousseau *et al.*, *Phys. Rev. Lett.*, 2001, **87**: 076101.